International Journal of Power Electronics and Drive System (IJPEDS)
Vol. 16, No. 4, December 2025, pp. 2296~2306
ISSN: 2088-8694, DOI: 10.11591/ijpeds.v16.i4.pp2296-2306

Design and analysis of brushless permanent magnet motor for light electrically powered two-wheeler vehicle

How Xuan Yu[1], Mohd Luqman Mohd Jamil[1,2], Nurul Ain Mohd Said[1,2]
[1]EV-PRODRIVES Research Group, Faculty of Electrical Technology and Engineering, Universiti Teknikal Malaysia Melaka, Melaka, Malaysia
[2]Department of Electrical Engineering, Faculty of Electrical Technology and Engineering, Universiti Teknikal Malaysia Melaka, Melaka, Malaysia

Article Info

Article history:

Received Mar 6, 2025
Revised Aug 6, 2025
Accepted Oct 17, 2025

Keywords:

Electric vehicle
Fractional-slot
Light electric vehicle
Power rating
Winding factor

ABSTRACT

This study provides a comprehensive process of designing an electric motor that will be used for a small two-wheeled electric vehicle. Due to high performance capability in term of power and torque, brushless permanent magnet topology is chosen so that a compromise between size constraint and performance can be met. For an accurate motor design sizing, the design process is initially carried out by determination of power rating that derived from vehicle dynamic calculation. Based on winding factor calculation, fractional-slot 12-slot/10-pole and 9-slot/10-pole motors equipped with non-overlapping winding are chosen and analyzed using finite element analysis (FEA) software. For an optimum electromagnetic performance, parametric optimization is included, mainly on the stator dimension. Despite the performance of both designs improved, only 9-slot motor results a convincing performance as the rated torque is 18% higher than the 12-slot design. For verification purpose, 1-D analytical solution is also included and compared with results deduced by the FEA. According to the analysis, the proposed motor designs are adequately reliable for a light electrically powered electric vehicle application.

Corresponding Author:

Mohd Luqman Mohd Jamil
EV-PRODRIVES Research Group, Faculty of Electrical Technology and Engineering
Universiti Teknikal Malaysia Melaka
Hang Tuah Jaya, Durian Tunggal, Melaka 76100, Malaysia
Email: luqman@utem.edu.my

1. INTRODUCTION

In systems or machinery where autonomous motion is required, electric motors are used to achieve desired mechanical action precisely. A brushed direct current (DC) motor was typically used for many applications in the past. The term DC comes as direct current, associated with the motor circuit that consists of field and armature windings. This motor topology needs a mechanical commutator to ensure a constant rotary direction exists. The armature winding on the rotor is connected to the power supply via a set of commutators and brushes. During the mechanical commutation, i.e. positive producing current, the magnetic field interaction between the field and armature results in a rotary motion. Common configurations of brushed DC motors are series, shunt and separately-excited systems. The separately-excited system inherently gives an advantage as the field winding, which is typically fed by an independent power supply, can be replaced by permanent magnets, especially when the motor size is relatively small [1]. Due to the nature of mechanical commutation, the control of DC motors is relatively simple [2]. However, the presence

of carbon brushes and commutator segments in a DC motor not only adds up to the maintenance cost, item, but also makes it less reliable [3].

On the other hand, brushless DC (BLDC) motors offer higher power density, efficiency, and reliability [4], [5]. These advantages result from the absence of brushes and a commutator. As the permanent magnets are mounted on the rotor while the windings are on the stator, electronic commutation provides alternating current to the windings, leading to varying magnetic fields. By using the same motor architecture, a specific switching control scheme applied on the inverter changes the brushless DC motor operation into a permanent magnet (PM) synchronous motor as the excitation current is sinusoidal. Although the PM synchronous motor (PMSM) has higher efficiency, is more capable for high speed, has lower output torque ripple, and less harmonics as compared to the BLDC motor, its control technique is more complex. Whereas a BLDC motor requires simpler control algorithms and is less demanding on position sensing precision, which contributes to lower cost [6].

For an alternating current (AC) driven system, induction motor and synchronous motor are common options. Both motors can operate on an AC source without the use of an inverter circuit. An AC synchronous motor offers the freedom to adjust both stator and field current, which allows better control and higher power density, but it still requires carbon brushes and slip rings, which poses the issue for low maintenance operation, besides having start-up and acceleration problems [7]-[9]. Meanwhile, for an induction motor, it has a simpler construction with no brushes and slip rings or commutator for squirrel cage rotor type [2], [10]. But the speed and torque are not easy to control due to their non-linear nature [3]. For a wound rotor induction motor, slip rings and brushes are still needed to excite the rotor windings, thus making it less commonly used. Another brushless motor type called switched reluctance motor (SRM) offers the advantage of simple construction, low rotor inertia, easy cooling, and outstanding torque-speed characteristics with the major drawback of acoustic noise and difficult control [4], [11].

BLDC motors are commonly utilized nowadays for several reasons. First, it is more efficient because it uses electronic commutation rather than mechanical commutation. It is achieved by relocating the armature windings to the stator while utilizing permanent magnet to provide magnetic field at rotor. Owing to the change to electronic commutation, BLDC motors can produce higher power density, which leads to higher torque to inertia ratio, in other words higher torque to rotor volume (TRV) ratio. Despite the advantages, its drive method is relatively simple, making BLDC a cost-effective option for many applications ranging from home appliances to various industrial machinery segments [12].

Electrification of road vehicles has been supported by policy makers worldwide to resolve environmental issues related to CO_2 emissions [13], and Malaysia is no exception. Apart from the government's effort, the market penetration of EVs is strongly dependent on battery costs [14], which makes up a big portion of the vehicles' total price. In addition, the acceptance of EV is also affected by the range, charging speed, and willingness of the public towards new product adoption [15]. Positively, a decline in battery cost will boost the EV environment [14]. A basic EV system is illustrated in Figure 1 [16], [17].

The trend of electrifying road vehicles has the upside of lowering air pollution and carbon footprints while also benefiting consumers and manufacturers. This is because the replacement of an internal combustion engine (ICE) with an EV system conceptually results in simple design architecture and minimum maintenance [18]. For lightweight EVs, the structure can be even simpler, cost-effective in production as well as consumer friendly. In developing countries, two-wheelers and hybrid electric vehicles (HEVs) have greater potential than four-wheeled EVs, according to a report in [15]. This is owing to the fact that electric two-wheelers are more affordable for the general public than four-wheeled EVs, i.e. rapid market penetration of electric two-wheeler in China [19]. Furthermore, electric 2-wheel (E2W) vehicles equipped with power-dense PM motors are more viable options as the efficiency trade-off for EVs is primarily mass-related [13]. Preview study [20], it is mentioned that the growth of EV necessitates the development of a high-performance motor.

In contrast to applications in manufacturing industries, traction motors must meet distinct operating parameters when chosen for an EV drivetrain. Wide speed range, good acceleration, great torque, especially at low speed, and high efficiency are often required of the motor [21]. PM motors are the most popular powertrain option among battery electric vehicles (BEVs), according to an analysis of 40 BEVs introduced between 2014 and 2016 (up to 26 models, or 65% of BEVs) [22]. Induction motors, synchronous reluctance motors, wound rotor synchronous motors, and other motor types are also used in EV drive systems. For an E2W design, a PM BLDC motor is used for the rear hub-mounted drivetrain because it has no excitation loss, fast dynamic response, and high efficiency [23]. A basic procedure to estimate accurate traction performance based on the vehicle dynamics, including the total vehicle weight, operating speed range, and road conditions, is presented.

In this study, the BLDC motor will be the main subject to be analyzed. Motors with several combinations of slot/pole will be designed and then simulated using finite element analysis (FEA) software. As the motors need to meet design requirements in terms of size and power, the initial design of each variant

is roughly made to match the size. Then a parametric optimization process takes place to obtain an optimum design for an optimum electromagnetic performance.

In FEA, the back electromotive force (EMF) of each design combination will be obtained. Besides, rated torque performance under static and dynamic current excitations will be examined. In addition to the FEA simulation, analytical solutions [24]-[27] are also employed to verify the proposed designs. This includes modelling the air gap flux-density under the influence of slot permeance to obtain phase back EMF and output torque, respectively.

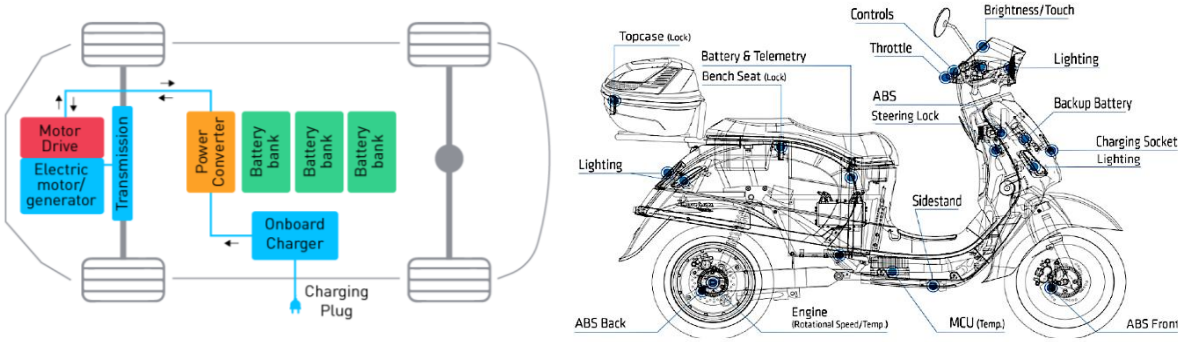

(a) (b)

Figure 1. Basic diagram of full electric vehicle system: (a) a four-wheeler electric vehicle system [16], and (b) a two-wheeler light electric vehicle system [17]

2. DESIGN AND ESTIMATION APPROACH

In order to design motors for specific applications, it is crucial to know the rating required to achieve the desired performance. Thus, this study starts off with motor rating determination, followed by stator and rotor design. For the case of a two-wheeler EV, motor sizing is very important, where motor axial length should be limited to fit within the width of the vehicle. In the case of a radial flux motor, the end winding overhang is the key contributor to the overall axial length of the motor. Therefore, fractional-slot concentrated windings are the best option for this application as they allow for improved design space by keeping the end winding smaller.

2.1. Vehicle dynamics calculation

The use of electric scooters and other lightweight electric two-wheelers is intended for comparatively slow commuting within cities; thus a comparatively low speed should be specified. In this case, Table 1 summarizes general specifications of the two-wheeler EV.

Table 1. General specifications for two-wheeler EV design

Parameter	Values
Tyre outer diameter	210 mm
Overall mass	150 kg
Maximum speed per hour	35 km/h
Tyre size	8.5 inch
Power train system	Direct-drives

2.1.1. Determination of mechanical capability

An output power, P_{mech} from a mechanical point of view is expressed as (1).

$$P_{mech} = \tau \times \omega_r \quad (1)$$

Where τ and ω are the output torque and angular velocity, which are in Nm and rad/s respectively. Using constants as tabulated in Table 2, the estimated power requirement of the electric motor were determined as Table 3. For a tyre with 210 mm outer diameter, the tyre circumference is 0.659 m. Thus, the vehicle's top speed of 35 km/h is translated into 884.19 rpm for a 1:1 transmission ratio, typically in a direct drive setup. It should be noted here that the use of velocity and speed is always interchangeable. There are three force components to be considered and summed together to meet the desired torque, namely rolling resistance

force, $F_{rolling}$, gradient load force, $F_{gradient}$ and aerodynamic drag, $F_{aerodynamic\ drag}$ as given in (2)-(4) [23]. All constants are tabulated in Table 2.

Besides the force, terrain conditions are also required to determine the required power rating. Based on [28], in town road design that is classified as arterial road will have maximum gradient ranging from 8% to 10%, which can be converted to angle using (5). Given a smooth paved road surface and a top speed of around 900 rpm for the vehicle, the $F_{gradient}$ component diminishes as the slope angle, θ equal to zero. On the other hand, to climb hills, the motor needs a higher output power to overcome the gradient force that increases as the road becomes steeper. Meanwhile, the speed requirement can be reduced under this condition. Considering the constants and design parameters, the torque and power under two different speed-slope operating conditions can be evaluated as in Table 3 using (1), (6), and (7). According to Table 3, the vehicle requires 643.6 W at 450 rpm and 329.1 W at 900 rpm when driven on uphill climbs and flat roads, respectively. The road conditions (slope, ideal, and uniform surface) potentially affect the developed power. Since the torque capability over a given speed results in produced power, the situation for both scenarios satisfy (1).

$$F_{rolling} = C_{rr} \times M \times g \tag{2}$$

$$F_{gradient} = M \times g \times sin\,\theta \tag{3}$$

$$F_{aerodynamic} = 0.5 C_D \times A_f \times \rho \times v^2 \tag{4}$$

$$road\ slope\ angle, \theta = tan^{-1} \frac{\%\ grade}{100} \tag{5}$$

$$F = F_{rolling} + F_{gradient} + F_{aerodynamic\ drag} \tag{6}$$

$$\tau = Fr \tag{7}$$

According to Table 3, the vehicle requires 643.6 W at 450 rpm and 329.1 W at 900 rpm when driven on uphill climbs and flat roads, respectively. The road conditions (slope and ideal uniform surface) potentially affect the developed power. Since the torque capability over a given speed results in produced power, the situation for both scenarios satisfy (1).

Table 2. Parameter consideration for torque determination

Parameter	Values
Coefficient of rolling resistance, C_{rr} (bicycle on asphalt road)	0.004
Gravitational constant, g (m/s^2)	9.81
Drag coefficient, C_d (for motorcycle with rider)	0.6
Frontal area, A_f (for motorcycle with rider)	0.8
Air density, ρ at 30° (kg/m^3)	1.1644

Table 3. Force, torque, and power calculations

Parameter	Top speed cruising	Uphill climb
$\%\ grade$	0 %	8 %
θ	0°	4.57°
$set\ speed$	900 rpm	450 rpm
$F_{rolling}$	5.886 N	5.886 N
$F_{gradient}$	0 N	117.345 N
$F_{aerodynamic}$	27.367 N	6.842 N
F_{total}	33.253 N	130.073 N
τ	3.492 Nm	13.658 Nm
P	329.1 W	643.6W

2.1.2. Motor design and sizing specifications

In this study, the motor size is fixed to 120 mm outer diameter and 48 mm axial length. The rotor topology is a surface-mounted permanent magnet (SPM), which rare-earth variant of NdFe35. This design is commonly employed to satisfy a design trade-off between magnetic performance, cost, and manufacturing constraints. Appropriate selection of slot/pole combination would result high winding factor, leading to better torque performance [28], [29]. To achieve an optimum electromagnetic performance, the size of the magnetic path has to be proportioned to a specified amount of flux density [30] as summarized in Table 4. The initial size of the stator back iron length, stator tooth width, and tooth tip width can then be determined using (8)-

(10), where θ_s , r_{si}, and w_{so} are slot pitch in radian, stator inner radius, and stator slot opening, respectively.

Other stator dimensions, i.e. tooth tip thickness, chamfer height, and slot base fillet radius can be selected without sacrificing too much slot depth. Whereas the slot depth is dependent on the split ratio selected and the stator outer diameter. For a radial flux PM motor, the optimum split ratio is between 0.6 and 0.7 [31]. For a given stator size, the rotor back iron thickness can be determined using (11). Since the 12-slot and 9-slot designs might require different rotor back iron thickness, an identical split ratio is considered here to allow two different stator slot numbers equipped with an identical rotor.

$$stator\ tooth\ width,\ w_{st} = \frac{B_{tt}}{B_{st}} w_{tt} \quad (8)$$

$$tooth\ tip\ width,\ w_{tt} = \theta_s r_{si} - w_{so} \quad (9)$$

$$stator\ back\ iron\ thickness,\ l_{sbi} = \frac{B_{st}}{B_{sbi}} w_{st} \quad (10)$$

$$rotor\ back\ iron\ thickness,\ l_{rbi} = \frac{B_{st}}{B_{rbi}} w_{st} \quad (11)$$

$$end\ winding\ length, l_e = \frac{\pi(D_{out} - 2l_{sbi})}{2N_s} \quad (12)$$

$$stator\ axial\ length, l_s = machine\ axial\ length - 2l_e \quad (13)$$

Figures 2(a) and 2(b) compare the 12-slot and 9-slot motor design layouts, while Figure 2(c) illustrates the machine dimension. To ensure an optimum size of stator casing, the end winding length can be approximated as a shape of half circle that spans across one slot pitch [30]. Thus, for an internal rotor motor, the end winding length can be defined as in (12). Then, the effective stator axial length can be determined using (13). Theoretically, the stator axial stack length for 12-slot motor is higher than the 9-slot motor. In this case, the stack length for 12-slot motor is 20 mm, while the 9-slot motor has a smaller size. Even though this may favour the 9-slot motor, the axial length of both motors is maintained at the same size in this study for a more convincing comparison and to enable both motors to use the same rotor. For the turn numbers and conductor size that relate to slot fill factor, a detailed calculation is analytically carried out by the associate program in Ansys software. Parametric optimization is then carried out on the designs within Ansys software to achieve the desired performance, giving the final design dimensions as tabulated in Table 5.

Table 4. Flux density distribution in stator and rotor components

Stator dimensions	Flux density (T)
Stator back iron, B_{sbi}	1.2
Stator tooth, B_{st}	1.8
Tooth tip, B_{tt}	0.9
Rotor back iron, B_{rbi}	1.4

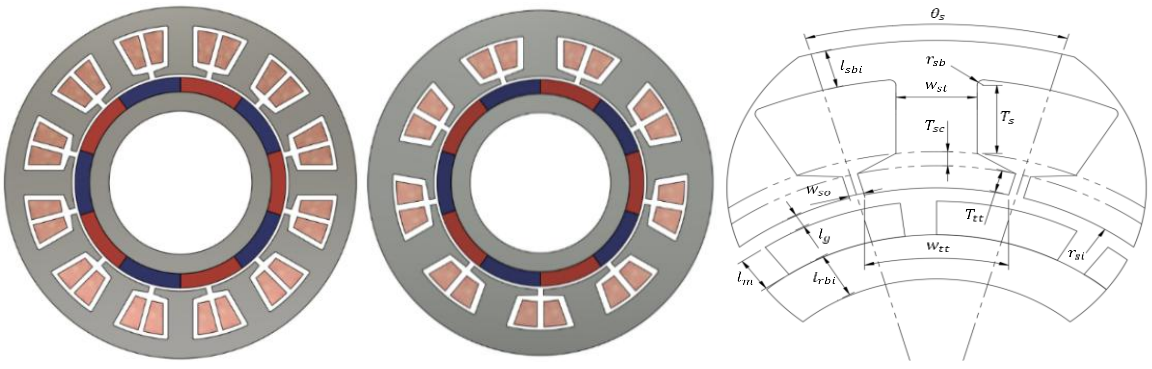

(a) (b) (c)

Figure 2. Design of RFPM motor with internal SPM rotor: (a) 12-slot 10-pole, (b) 9-slot 10-pole, and (c) geometry dimension

Table 5. Design specifications

Parameter	12-slot design	9-slot design	Parameter	12-slot design	9-slot design
Slot/pole combination	$N_s \pm 2$	$N_s \pm 1$	Slot base fillet radius, r_{sb}	0.6 mm	0.6 mm
DC bus voltage, V_{dc}	48 V	48 V	Slot chamber height, T_{sc}	3.3mm	2.6 mm
Rated speed, ω_r	450 rpm	450 rpm	Slot depth, T_s	9.7 mm	10.1 mm
Rated power, P	650 W	650 W	Stator axial length, l_s	20 mm	20 mm
Air gap thickness, l_q	1 mm	1 mm	Coil turn numbers, N_{coil}	37	46
Slot number, N_s	12	9	Pole numbers, $2p$	10	10
Stator outer diameter, D_{so}	120 mm	120 mm	Pole embrace	1	1
Stator inner diameter, D_{si}	74 mm	74 mm	Rotor outer diameter, D_{ro}	72 mm	72 mm
Split ratio, λ	0.6167	0.6167	Rotor inner diameter, D_{ri}	48.8 mm	48.8 mm
Stator slot opening, w_{so}	2 mm	2.2 mm	Rotor back iron thickness, l_{rbi}	6.6 mm	6.6 mm
Stator tooth width, w_{st}	7.4 mm	10.1 mm	Magnet thickness, l_m	5 mm	5 mm
Stator back iron thickness, l_{sbi}	7.3 mm	8.6 mm	Rotor axial length, l_r	20 mm	20 mm
Tooth tip thickness, T_{tt}	2.1 mm	1.1 mm			

2.2. Analytical solutions

In analytical modelling, airgap flux density of PM motor is first derived using equations from [24], [25]. The radial component of the airgap flux density is modelled for an internal rotor motor since it is the normal component of the magnetic field provided by magnets on the rotor that directly interacts with the stator. Considering the slotting effect of stator, [26] provided the permeance function to model the effect of slotting toward airgap flux, enabling more accurate prediction. Besides, a detailed implementation of the relative permeance function was made referring to the method used in [31].

With known airgap flux density, the phase back EMF of the motor can be modelled for PM motor with a selected slot pole combination. Note that only the average relative permeance is considered in the equation of back EMF based on [27]. Subsequently, output torque can be modelled by (14) using the back EMF obtained analytically. For the case of BLDC operation, the currents are excited in a trapezoidal shape with 120° electrical conduction angle, which has to be modelled separately using a piecewise function to obtain the torque waveform. E_a, E_b, E_c are the phase back EMFs, while i_a, i_b, i_c these are the phase currents.

$$output\ torque, \tau = \frac{E_a i_a + E_b i_b + E_c i_c}{\omega_r} \quad (14)$$

3. RESULTS AND ANALYSIS

3.1. Open-circuit flux density

Open circuit flux densities for the 12-slot and 9-slot optimized final motors are shown in Figure 3, where the prediction using FEA peaks is around 0.85 T. The little dented peak in every positive and negative part is due to the influence of slot-opening. Figures 3(a) and 3(b) confirm that the simulated FEA and analytical solution results are in good agreement. Besides, the dip in flux density magnitude for both motors indicates that the stator slotting effect is modeled correctly by the analytical method.

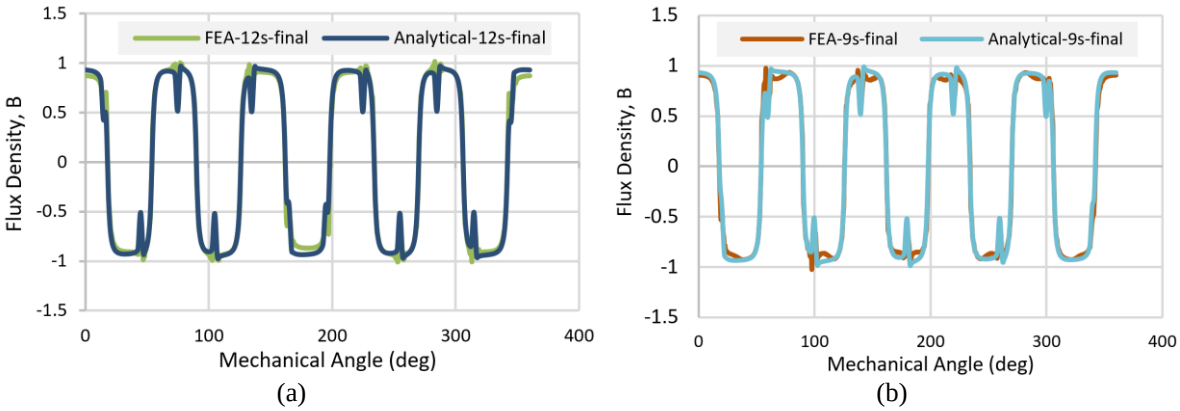

Figure 3. Open circuit flux densities: (a) FEA vs analytical results for 12-slot motor, and (b) FEA vs analytical results for 9-slot motor

3.2. Back EMF

Figure 4 compares results extracted from the FEA and analytical methods for the phase back EMF. It is shown in non-linear FEA simulation that the 12-slot motor results sinusoidal phase back EMF while the 9-slot motor results a more trapezoidal shape, as shown in Figure 4. This phenomenon is due to the rise of multiple harmonics order in the 9-slot design. For both slot pole combinations, the linear condition results are in better agreement with analytical solutions.

Table 6 summarizes the root mean square (RMS) values of the phase back EMF. Due to the nature of analytical solution, the back EMF magnitudes are closer to that of FEA under linear condition. As the linear condition is relatively ideal due to non-saturation effect, higher phase back EMF exists in both 12-slot and 9-slot designs.

Table 6. RMS phase back EMF

Method	12-slot		9-slot	
	Non-linear	Linear	Non-linear	Linear
FEA	6.40	7.73	6.61	7.36
Analytical	-	7.64	-	8.1

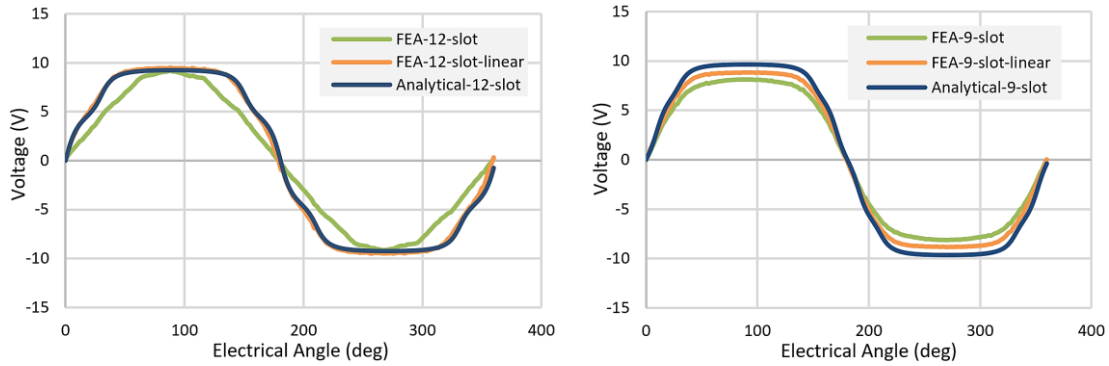

Figure 4. Phase back EMFs: (a) FEA linear and non-linear condition vs analytical results for 12-slot motor, and (b) FEA linear and non-linear condition vs analytical results for 9-slot motor

3.3. Dynamic torque and current

Figure 5(a) compares the output torque when the motor runs in BLDC mode with an implementation of six-step commutation. It should be noted that the motor is virtually driven by an ideal inverter whose DC bus voltage is 48 V. The motor is inherently excited by a current in each phase, as shown in Figure 5(b). It is shown that the 12-slot motor produces lesser torque while drawing more current than its 9-slot counterpart. This can be due to the influence of variation of saturation level and losses. Back to Figure 5(b), the current waveforms appear to be the same shape. It is commonly known that the fishbone type of the excitation current is due to the effect of winding inductance and phase switching sequence among phases.

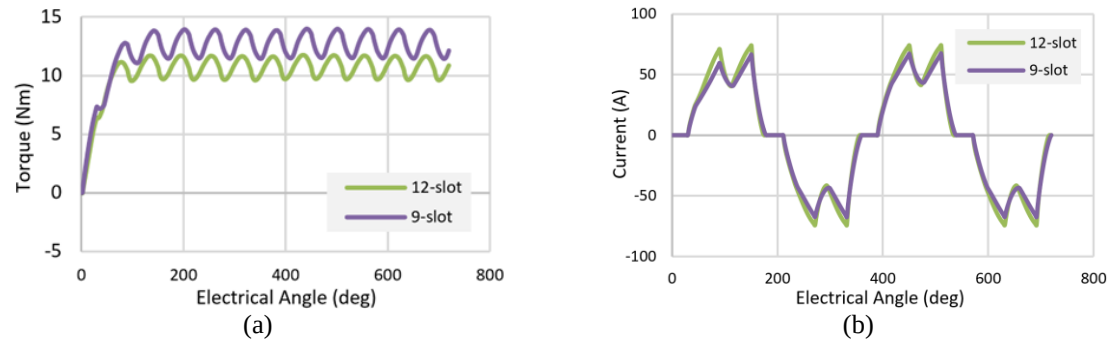

Figure 5. FEA dynamic simulation: (a) output torque, and (b) phase excitation current

Table 7 summarize the motor output torque and current drawn from the inverter. From the result, 9-slot design produce 18.1% higher torque while requiring 7.4% less phase current. Hence, the 9-slot design is more advantageous for torque demanding application, such as high-performance electric two-wheeler.

Table 7. Output torque and phase current values at steady-state

Parameter	12-slot	9-slot
Average torque (Nm)	10.75	12.74
Peak-to-peak torque (Nm)	2.14	2.55
Torque ripple (%)	19.86	19.98
RMS phase current (A)	45.88	42.47

3.4. Static torque and current

Theoretically, an ideal trapezoidal phase current leading to an ideal output torque produced by the motor can be simply modelled. This is done by setting the peak value identical to the RMS value of the excitation current drawn from the inverter in dynamic conditions. Figure 6 compares the static output torque calculated using both methods.

According to Figure 6, the 9-slot motor is found to have a smaller torque ripple and a higher torque than the 12-slot motor. In theory, this results in reduced vibration even though the phase winding is asymmetrically disposed. Figures 6(a) and 6(b) respectively compare the results obtained using both methods in the respective motors. The analytical method generally estimated a higher average torque than FEA simulations. Besides, the shape of the torque ripple is more uniform and symmetry, which is not slanted to one side as observed in FEA results. This is because the saturation condition in the magnetic iron path is not considered in analytical solutions. Instead, just one point in the material's B-H curve's permeability is taken into account, and the motor's actual dimensions are not taken into account by the entirely computational equation. Table 8 summarizes the performance of the output torque at rated condition. From Table 8, the FEA results shows that the 9-slot final design achieved 10.1% higher average torque while having 56.3% reduction in torque ripple percentage. This again shows that 9-slot design is better for high torque scenario.

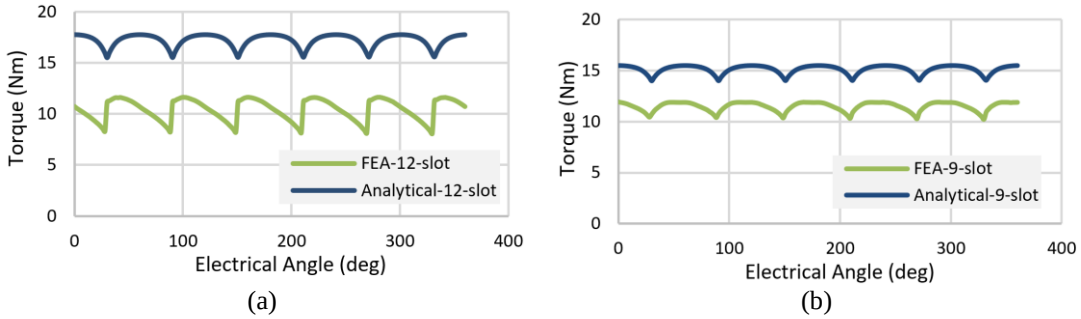

Figure 6. Output torque in static condition: (a) FEA vs analytical results for 12-slot motor, and (b) FEA vs analytical results for 9-slot motor

Table 8. Output torque performances

Parameter	12-slot		9-slot	
	FEA	Analytical	FEA	Analytical method
Average torque (Nm)	10.44	17.22	11.50	15.11
Peak-to-peak torque (Nm)	3.55	2.23	1.71	1.49
Torque ripple (%)	33.99	12.98	14.83	9.88

3.4.1. Cogging torque

Figure 7 compares the cogging torque of both motors using FEA. The cogging effect is resulted by the natural attraction and repulsion between the rotor magnets and the stator iron. In comparison to the 9-slot motor, the 12-slot motor has a larger amplitude but fewer cogging cycles based on the theorem of smallest common multiple, N_{scm}. This is illustrated in Figure 7(a), where the simulation is made under linear condition without saturation of core iron. However, the cogging torque for 12-slot motor is significantly lower under non-linear condition as seen in Figure 7(b). Table 9 recorded the cogging torque magnitude by

peak-to-peak value for both 12-slot and 9-slot design under linear and non-linear condition. The cogging torque magnitude of 9-slot motor is doubled compared to 12-slot motor in non-linear condition.

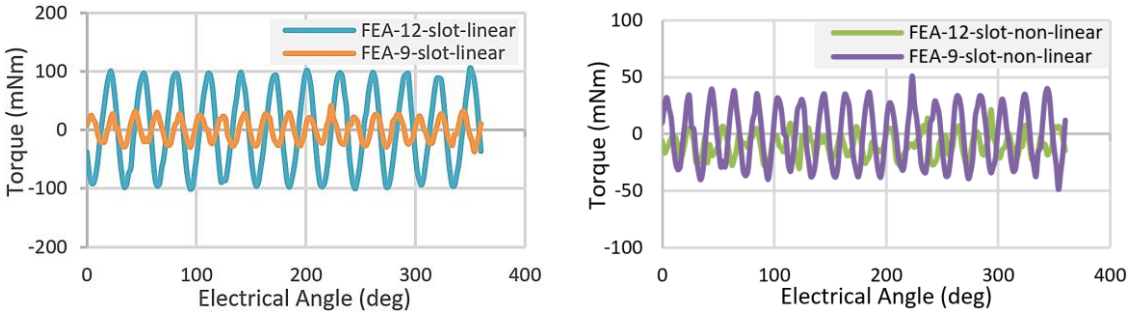

(a) (b)

Figure 7. Cogging torque via FEA: (a) 12-slot vs 9-slot motor: linear condition, and (b) 12-slot vs 9-slot motor: non-linear condition

Table 9. Cogging torque magnitudes

Parameter	12-slot	9-slot
Cogging torque, non-linear (Nm)	0.05	0.10
Cogging torque, linear (Nm)	0.21	0.08
Number of cycles	60	90

4. CONCLUSION

In this study, a detailed design and analysis of three-phase permanent magnet motor having identical rotor but different slot numbers for a light electric two-wheeler vehicle is presented. The combination of slot number and pole results the employment of fractional-slot winding with concentrated coils. The design begins with calculation of force components for rolling vehicle leading to an accurate motor's power rating requirement. From machine design perspective, the fixed outer size limits motor capability to be achieved thus an optimization process is implemented and results significant achievement of intended power. Although the initial results of parametric optimization show improvement in performance, further evaluation was done by implementing an ideal inverter drives in FEA where the electromagnetic characteristics, such as open-circuit flux density, back EMF and output torque, which are then calculated and validated by the analytical formula. Based on the flux density waveforms, analytical solution and FEA results are in a good agreement. The FEA approach shows that the 9-slot and 12-slot motors having similar phase back EMFs. The underlying difference between analytical and FEA methods can be clearly seen within the static torque result, as the analytical method predicted higher output torque due to the factor of linear operating condition. Through static and dynamic analyses, the 9-slot motor demonstrates a better performance of output torque than the 12-slot motor with a relative increment of 18%. Despite, the 9-slot motor results bigger cogging torque than the 12-slot motor under non-linear condition. At rated speed of 450 rpm, the 9-slot motor achieved 12.74 Nm torque dynamically which corresponds to the desired power of 600 W. This is adequately reliable, even the initial aim was 650 W. It is essential to highlight that the developed motors in this research theoretically can serve as the powertrain for a lightweight electric vehicle.

FUNDING INFORMATION

The authors would like to thank Universiti Teknikal Malaysia Melaka (UTeM) for providing UTeM Kesidang Scholarship and Ministry of Higher Education (MOHE) for continuous support of research development under national grant scheme, FRGS/1/2024/TK07/UTEM/02/13.

AUTHOR CONTRIBUTIONS STATEMENT

This journal uses the Contributor Roles Taxonomy (CRediT) to recognize individual author contributions, reduce authorship disputes, and facilitate collaboration.

Name of Author	C	M	So	Va	Fo	I	R	D	O	E	Vi	Su	P	Fu
How Xuan Yu	✓	✓	✓			✓		✓	✓		✓			
Mohd Luqman Mohd Jamil	✓	✓		✓	✓	✓	✓	✓	✓	✓		✓	✓	✓
Nurul Ain Mohd Said	✓			✓			✓	✓	✓	✓		✓		

C : **C**onceptualization
M : **M**ethodology
So : **So**ftware
Va : **Va**lidation
Fo : **Fo**rmal analysis
I : **I**nvestigation
R : **R**esources
D : **D**ata Curation
O : Writing - **O**riginal Draft
E : Writing - Review & **E**diting
Vi : **Vi**sualization
Su : **Su**pervision
P : **P**roject administration
Fu : **Fu**nding acquisition

CONFLICT OF INTEREST STATEMENT

Authors state no conflict of interest.

DATA AVAILABILITY

The data that support the findings of this study are available from the corresponding author, [MLMJ], upon reasonable request.

REFERENCES

[1] S.-H. Kim, "Control of direct current motors," in *Electric Motor Control*, Elsevier, 2017, pp. 39–93. doi: 10.1016/B978-0-12-812138-2.00002-7.

[2] J. F. Gieras, *Permanent magnet motor technology*. 2009.

[3] M. A. Hannan, J. A. Ali, A. Mohamed, and A. Hussain, "Optimization techniques to enhance the performance of induction motor drives: A review," *Renewable and Sustainable Energy Reviews*, vol. 81, pp. 1611–1626, Jan. 2018, doi: 10.1016/j.rser.2017.05.240.

[4] K. T. Chau, C. C. Chan, and L. Chunhua, *Overview of permanent-magnet brushless drives for electric and hybrid electric vehicles*. 2008. doi: 10.1109/TIE.2007.918403.

[5] J. F. Gieras, R. J. Wang, and M. J. Kamper, "Axial flux permanent magnet brushless machines," *Axial Flux Permanent Magnet Brushless Machines*, pp. 1–340, 2005, doi: 10.1007/1-4020-2720-6.

[6] S. Sakunthala, R. Kiranmayi, and P. N. Mandadi, "A study on industrial motor drives: Comparison and applications of PMSM and BLDC motor drives," in *2017 International Conference on Energy, Communication, Data Analytics and Soft Computing, ICECDS 2017*, 2018, pp. 537–540. doi: 10.1109/ICECDS.2017.8390224.

[7] N. N. Siphepho and K. S. Garner, "Design and performance analysis of a dual three phase large scale wound rotor synchronous machine," in *2022 International Conference on Electrical Machines (ICEM)*, Sep. 2022, pp. 206–211. doi: 10.1109/ICEM51905.2022.9910813.

[8] S. S. H. Bukhari, G. J. Sirewal, M. Ayub, and J.-S. Ro, "A new small-scale self-excited wound rotor synchronous motor topology," *IEEE Transactions on Magnetics*, vol. 57, no. 2, pp. 1–5, Feb. 2021, doi: 10.1109/TMAG.2020.3009372.

[9] M. Fadel, S. Caux, G. Borghetti, and G. Postiglione, "Sensorless starting of wound rotor synchronous machines," in *2019 21st European Conference on Power Electronics and Applications, EPE 2019 ECCE Europe*, 2019. doi: 10.23919/EPE.2019.8915211.

[10] S.-H. Kim, "Alternating current motors," in *Electric Motor Control*, Elsevier, 2017, pp. 95–152. doi: 10.1016/B978-0-12-812138-2.00003-9.

[11] A. M. Dharne and P. L. B. Awale, "Analysis of switched reluctance motor performance with different slot pole combinations," *International Journal for Research in Applied Science and Engineering Technology*, vol. 10, no. 6, pp. 2158–2164, Jun. 2022, doi: 10.22214/ijraset.2022.44201.

[12] S.-H. Kim, "Brushless direct current motors," in *Electric Motor Control*, Elsevier, 2017, pp. 389–416. doi: 10.1016/B978-0-12-812138-2.00010-6.

[13] M. Weiss, K. C. Cloos, and E. Helmers, "Energy efficiency trade-offs in small to large electric vehicles," *Environmental Sciences Europe*, vol. 32, no. 1, p. 46, Dec. 2020, doi: 10.1186/s12302-020-00307-8.

[14] J. Krause *et al.*, "EU road vehicle energy consumption and CO2 emissions by 2050 – Expert-based scenarios," *Energy Policy*, vol. 138, p. 111224, Mar. 2020, doi: 10.1016/j.enpol.2019.111224.

[15] S. Z. Rajper and J. Albrecht, "Prospects of electric vehicles in the developing countries: a literature review," *Sustainability*, vol. 12, no. 5, p. 1906, Mar. 2020, doi: 10.3390/su12051906.

[16] Monolithic Power Systems, "Power electronic for electric vehicles," *MPS*, 2025.

[17] N. Schelte, S. Severengiz, J. Schünemann, S. Finke, O. Bauer, and M. Metzen, "Life cycle assessment on electric moped scooter sharing," *Sustainability*, vol. 13, no. 15, p. 8297, Jul. 2021, doi: 10.3390/su13158297.

[18] F. Alanazi, "Electric vehicles: benefits, challenges, and potential solutions for widespread adaptation," *Applied Sciences*, vol. 13, no. 10, p. 6016, May 2023, doi: 10.3390/app13106016.

[19] M. Weiss, P. Dekker, A. Moro, H. Scholz, and M. K. Patel, "On the electrification of road transportation – A review of the environmental, economic, and social performance of electric two-wheelers," *Transportation Research Part D: Transport and Environment*, vol. 41, pp. 348–366, Dec. 2015, doi: 10.1016/j.trd.2015.09.007.

[20] B. D. S. G. Vidanalage, S. Mukundan, W. Li, and N. C. Kar, "An overview of PM synchronous machine design solutions for enhanced traction performance," in *2020 International Conference on Electrical Machines (ICEM)*, Aug. 2020, pp. 1697–1703. doi: 10.1109/ICEM49940.2020.9270882.

[21] M. S. Patil and S. S. Dhamal, "A detailed motor selection for electric vehicle traction system," in *Proceedings of the 3rd International Conference on I-SMAC IoT in Social, Mobile, Analytics and Cloud, I-SMAC 2019*, 2019, pp. 679–684. doi: 10.1109/I-SMAC47947.2019.9032616.
[22] E. A. Grunditz and T. Thiringer, "Performance analysis of current BEVs based on a comprehensive review of specifications," *IEEE Transactions on Transportation Electrification*, vol. 2, no. 3, pp. 270–289, Sep. 2016, doi: 10.1109/TTE.2016.2571783.
[23] M. S. Khande, A. S. Patil, G. C. Andhale, and R. S. Shirsat, "Design and development of electric scooter," *Energy*, vol. 40, no. 60, p. 100, 2020.
[24] Z. Q. Zhu, D. Howe, E. Bolte, and B. Ackermann, "Instantaneous magnetic field distribution in brushless permanent magnet DC motors, Part I: open-circuit field," *IEEE Transactions on Magnetics*, vol. 29, no. 1, pp. 124–135, 1993.
[25] Z. Q. Zhu and D. Howe, "Instantaneous magnetic field distribution in brushless permanent magnet DC motors, Part II: armature-reaction field," *IEEE Transactions on Magnetics*, vol. 29, no. 1, pp. 136–142, 2002.
[26] Z. Q. Zhu and D. Howe, "Instantaneous magnetic field distribution in brushless permanent magnet DC motors, Part III: effect of stator slotting," *IEEE Transactions on Magnetics*, vol. 29, no. 1, pp. 143–151, 2002.
[27] Z. Q. Zhu and D. Howe, "Instantaneous magnetic field distribution in permanent magnet brushless DC motors, Part IV: magnetic field on load," *IEEE Transactions on Magnetics*, vol. 29, no. 1, pp. 152–158, 2002.
[28] R. Robinson and B. Thagesen, *Road engineering for development*. London, 2004. doi: 10.4324/9780203301982.
[29] M. N. Othman, "Design and evaluation of high power density brushless DC permanent magnet machines," University of Nottingham, 2012.
[30] F. Chai, Y. Bi, and L. Chen, "A comparison between axial and radial flux permanent magnet in-wheel motors for electric vehicle," in *2020 International Conference on Electrical Machines (ICEM)*, Aug. 2020, pp. 1685–1690. doi: 10.1109/ICEM49940.2020.9270905.
[31] M. Olszewski, "Fractional-slot surface mounted PM motors with concentrated windings for HEV traction drives," *Energy Efficiency and Renewable Energy FreedomCAR and Vehicle Technologies, Vehicle Systems Team*, 2005, [Online]. Available: http://www.osti.gov/energycitations/product.biblio.jsp?osti_id=885979

BIOGRAPHIES OF AUTHORS

How Xuan Yu was born in Melaka, Malaysia, in 1999 and received the B.Eng. degree in Electrical Engineering from Universiti Teknikal Malaysia Melaka Malaysia (UTeM) in 2023. He is currently pursuing his Master of Science at Universiti Teknikal Malaysia Melaka, Malaysia. He can be contacted at email: xyhow1234@gmail.com.

Mohd Luqman Mohd Jamil obtained his B.Eng. degree from Universiti Teknologi MARA, Shah Alam, Malaysia, in 2000, followed by an M.Sc. from University of Newcastle upon Tyne, United Kingdom, in 2003, and a Ph.D. from The University of Sheffield, United Kingdom, in 2011, all in electrical engineering. He serves as a lecturer at the Faculty of Electrical Technology and Engineering, University Teknikal Malaysia Melaka, Malaysia. His research is interests include design, analysis, and control of electric machines. He can be contacted at email: luqman@utem.edu.my.

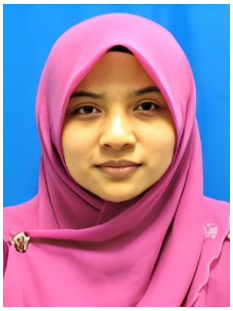

Nurul Ain Mohd Said received the B.Eng. and the M.Sc. degrees from Universiti Teknologi Malaysia, Skudai, Malaysia, in 2009 and University of Strathclyde, Glasgow in 2011, respectively, and the Ph.D. degree from University of New South Wales, Sydney, Australia, in 2017, all in electrical engineering. She is currently a senior lecturer at the Faculty of Electrical Technology and Engineering, University Teknikal Malaysia Melaka, Melaka, Malaysia. Her research interests include power electronics, drives, and energy conversion. She can be contacted at email: nurulain@utem.edu.my.